Time-Reversal-Violating Photonic Topological Insulators with Helical Edge States

Tetsuyuki Ochiai

Photonic Materials Unit, National Institute for Materials Science (NIMS), Tsukuba, Ibaraki 305-0044, Japan

We theoretically demonstrate the realization of photonic topological insulators in photonic crystals made of circular cylinders with the Tellegen-type magnetoelectric coupling as a photospin-orbit interaction. Although the magnetoelectric coupling breaks the conventional (bosonic) time-reversal symmetry for photons, the electromagnetic duality between permittivity and permeability gives rise to a fermionic time-reversal symmetry. This symmetry along with the space-inversion symmetry enables us to imitate the Kane-Mele model of two-dimensional topological insulators in a photonics platform. Even if the space-inversion symmetry is broken, a photonic topological insulator can emerge owing to the photospin-orbit interaction. We present bulk and edge properties of the photonic topological insulators and discuss their possible realization.

1. Introduction

Topology plays a major role in current condensed matter physics. The quantum Hall effect and topological insulator (TI) are two landmarks that highlight topology in momentum space.[1,2] Inspired by these two topics, recently, much attention has been paid to topological phenomena of photons in photonic crystals (PhCs), metamaterials, and coupled cavity arrays. They include Hall effect of light,[3] optical one-way waveguide,[4,5] photonic analog of fractional quantum Hall effect,[6] photonic TI (PTI),[7–9] photonic Floquet TI,[10] and synthetic gauge field for photons.[11,12] Although many of these phenomena are yet theoretical proposals, their experimental verification has made substantial progress recently.[13]

Here, we pick up a PTI proposed by Khanikaev et al.[8] They studied a photonic analog of the two-dimensional TI in a certain PhC. It consists of a periodic array of metamaterial rods with an effective off-diagonal magnetoelectric (ME) coupling of the Pasteur type.[14] The ME coupling acts as a spin-orbit interaction for light. This coupling is an extension of the so-called Drude-Born-Fedorov chirality[15] and preserves the time-reversal symmetry (TRS). The PhC structure in their proposal is a metacrystal with multi-dimensional spatial periodicity with two different length scales: One is a constituent metamaterial rod with a subwavelength periodic structure of split-ring resonators. The other is a PhC itself composed of the metamaterial rods. A sophisticated design of the effective ME coupling along with the electromagnetic duality between permittivity and permeability is necessary.

To avoid the metamaterial design of the ME coupling, another medium can be considered. It is a Tellegen medium, which has an ME coupling without the TRS.[16] A multiferroic material is a typical example of the Tellegen medium, and can have various forms of the ME tensor.[17] Composites of the piezoelectric and piezomagnetic media also exhibit an effective ME coupling through mechanical strain.[18,19] In the former case, the ME coupling is built-in and has a strong frequency dependence. In the latter case, the coupling can be controlled by a Bragg stack with one-dimensional periodicity. Again, it has a strong frequency dependence. Multi-dimensional periodicity such as in the split-ring resonator array is not required for these ME couplings.

Introducing such an ME coupling without the TRS seems to contradict with PTI, because the usual TI is protected by the TRS. In fact, the resulting (electronic) helical edge states of TI and their robustness depend strongly on the Kramers degeneracy due to the TRS. Although the TRS (and parities) is broken by the ME coupling of the Tellegen type, we can demonstrate a realization of PTI with the help of the electromagnetic duality and resulting fermionic TRS, as shown by He et al. very recently for a square lattice.[20] The electromagnetic duality between permittivity and permeability is a key item in this construction of PTI, and we require a sophisticated design for the duality as in the metamaterial construction.

In this work, we develop and strengthen this idea, studying a wider class of PhCs with and without the space-inversion symmetry (SIS). Notions of effective hamiltonians are also introduced. The Kramers degeneracy due to the fermionic TRS and the photospin-orbit interaction by the ME coupling enable us to construct PTIs. If the SIS is preserved in the PhCs, the system can be mapped to the Kane-Mele model.[21] Even if the SIS is broken, the system can exhibit PTI, as predicted by an effective hamiltonian. These predictions are numerically verified by evaluating edge states for various edge configurations.

This paper is organized as follows. In Sect. 2, we define our PhCs and discuss their symmetry properties. Section 3 is devoted to presenting the effective hamiltonian around quartic-degenerate modes at Γ and K(K') points in the first Brillouin zone of the triangular-, honeycomb-, and kagome-lattice PhCs. In Sect. 4, we study edge states in the PhCs, and helical edge states are shown to emerge in accordance with the effective hamiltonian along with the Z_2 indices calculated from the photonic band structures. In Sect. 5, summary and discussions are given.

2. Photonic Crystals Made of Magnetoelectric Media

Let us consider a uniaxial optical substance with the ME coupling. We assume the following constitutive relation for the electric displacement $\boldsymbol{D}$ and the magnetic field $\boldsymbol{H}$:

$$\boldsymbol{D} = \epsilon_0 \overleftrightarrow{\epsilon} \boldsymbol{E} + \overleftrightarrow{\chi} \boldsymbol{B}, \tag{1}$$

$$\boldsymbol{H} = (\mu_0 \overleftrightarrow{\mu})^{-1} \boldsymbol{B} - \overleftrightarrow{\chi}^t \boldsymbol{E}, \tag{2}$$

$$\overleftrightarrow{\epsilon} = \mathrm{diag}(\epsilon_p, \epsilon_p, \epsilon_z), \tag{3}$$

$$\overleftrightarrow{\mu} = \mathrm{diag}(\mu_p, \mu_p, \mu_z), \tag{4}$$

$$\overleftrightarrow{\chi} = \begin{pmatrix} \chi_p & \chi_o & 0 \\ -\chi_o & \chi_p & 0 \\ 0 & 0 & \chi_z \end{pmatrix}. \tag{5}$$

Such an ME coupling $\overleftrightarrow{\chi}$ appears most typically in multiferroic materials, through the cross term $\chi_{ij}E_iB_j$ in the effective Lagrangian. For simplicity, we assume real $\overleftrightarrow{\epsilon}$, $\overleftrightarrow{\mu}$, and $\overleftrightarrow{\chi}$ to make the system dissipationless. In what follows, we assume a frequency-independent large ME coupling for numerical simulations. Since the ME coupling generally has a strong frequency dependence via a resonance, the assumption is justified only for a narrow frequency range near the resonance. Taking account of the scale invariance in the Maxwell equation, a numerical result of wide frequency interval should be interpreted as a collection of patches. Each patch covers a narrow frequency range, and among different patches, the length scales (or the lattice constants of the PhCs) are different.

The system breaks the conventional (and bosonic) TRS $\mathcal{T}_b$. The radiation field behaves under the time reversal as

$$\boldsymbol{E} \to \boldsymbol{E}^*, \tag{6}$$

$$\boldsymbol{B} \to -\boldsymbol{B}^*, \tag{7}$$

$$\boldsymbol{D} \to \boldsymbol{D}^*, \tag{8}$$

$$\boldsymbol{H} \to -\boldsymbol{H}^*. \tag{9}$$

Here, the harmonic time dependence of the field is assumed, namely,

$$\boldsymbol{F}(t) = \Re[\boldsymbol{F}e^{-i\omega t}] \quad (\boldsymbol{F} = \boldsymbol{E}, \boldsymbol{B}, \boldsymbol{D}, \boldsymbol{H}). \tag{10}$$

Under $\mathcal{T}_b$, the constitutive relation for $\boldsymbol{D}$ becomes

$$\boldsymbol{D}^* = \epsilon_0 \overleftrightarrow{\epsilon}\boldsymbol{E}^* - \overleftrightarrow{\chi}\boldsymbol{B}^*, \tag{11}$$

which contradicts the complex conjugation of Eq. (1). Therefore, real $\overleftrightarrow{\chi}$ breaks the TRS. The ME coupling also breaks parity symmetries, because the electric and magnetic fields are vector and axial-vector, respectively.[22] Note that the rotational symmetry with respect to the z-axis is preserved under the assumption of Eqs. (3)-(5).

Although the constitutive relation of Eqs. (1) and (2) is natural, it is convenient to rewrite the relation as

$$\boldsymbol{D} = \epsilon_0 \overleftrightarrow{\epsilon}^{\mathrm{EH}}\boldsymbol{E} + \overleftrightarrow{\chi}^{\mathrm{EH}}\boldsymbol{H}, \tag{12}$$

$$\boldsymbol{B} = \mu_0 \overleftrightarrow{\mu}^{\mathrm{EH}}\boldsymbol{H} + (\overleftrightarrow{\chi}^{\mathrm{EH}})^t\boldsymbol{E}, \tag{13}$$

$$\overleftrightarrow{\epsilon}^{\mathrm{EH}} = \mathrm{diag}(\epsilon_p^{\mathrm{EH}}, \epsilon_p^{\mathrm{EH}}, \epsilon_z^{\mathrm{EH}}), \tag{14}$$

$$\overleftrightarrow{\mu}^{\mathrm{EH}} = \mathrm{diag}(\mu_p^{\mathrm{EH}}, \mu_p^{\mathrm{EH}}, \mu_z^{\mathrm{EH}}), \tag{15}$$

$$\overleftrightarrow{\chi}^{\mathrm{EH}} = \begin{pmatrix} \chi_p^{\mathrm{EH}} & \chi_o^{\mathrm{EH}} & 0 \\ -\chi_o^{\mathrm{EH}} & \chi_p^{\mathrm{EH}} & 0 \\ 0 & 0 & \chi_z^{\mathrm{EH}} \end{pmatrix}, \tag{16}$$

$$\epsilon_p^{\mathrm{EH}} = \epsilon_p + \frac{\mu_0}{\epsilon_0}\mu_p(\chi_p^2 + \chi_o^2), \quad \epsilon_z^{\mathrm{EH}} = \epsilon_z + \frac{\mu_0}{\epsilon_0}\mu_z\chi_z^2, \tag{17}$$

$$\mu_p^{\mathrm{EH}} = \mu_p, \quad \mu_z^{\mathrm{EH}} = \mu_z, \tag{18}$$

$$\chi_p^{\mathrm{EH}} = \mu_0\mu_p\chi_p, \quad \chi_o^{\mathrm{EH}} = \mu_0\mu_p\chi_o, \quad \chi_z^{\mathrm{EH}} = \mu_0\mu_z\chi_z. \tag{19}$$

The electromagnetic duality becomes simplified in this notation, because $\boldsymbol{E}$ and $\boldsymbol{H}$ (or $\boldsymbol{D}$ and $\boldsymbol{B}$) fields are formally similar in the Maxwell equation. The duality is simply defined by $\overleftrightarrow{\epsilon}^{\mathrm{EH}} = \overleftrightarrow{\mu}^{\mathrm{EH}}$.

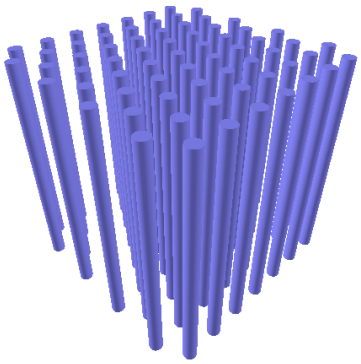

Fig. 1. (Color online) Schematic illustration of the system under study. It consists of a periodic array of magnetoelectric cylinders with circular cross sections.

Suppose we have a parallel array of the ME rods arranged periodically in the background medium. The background medium is supposed to have scalar permittivity, permeability, and vanishing ME coupling. Figure 1 shows a schematic illustration of the system under study. We now restrict ourselves to in-plane (the xy plane) light propagation perpendicular to the rod axis (the z-direction). The Maxwell equation now reduces to the following two-component equation for E_z and H_z:

$$\begin{pmatrix} -\boldsymbol{\nabla}\cdot(\xi\boldsymbol{\nabla}*) & -\boldsymbol{\nabla}\cdot(\tilde{\chi}_p\boldsymbol{\nabla}*) + [\boldsymbol{\nabla}\times(\tilde{\chi}_o\boldsymbol{\nabla}*)]_z \\ -\boldsymbol{\nabla}\cdot(\tilde{\chi}_p\boldsymbol{\nabla}*) - [\boldsymbol{\nabla}\times(\tilde{\chi}_o\boldsymbol{\nabla}*)]_z & -\boldsymbol{\nabla}\cdot(\eta\boldsymbol{\nabla}*) \end{pmatrix} \times \begin{pmatrix} \sqrt{\epsilon_0}E_z \\ \sqrt{\mu_0}H_z \end{pmatrix} = \frac{\omega^2}{c^2}\begin{pmatrix} \epsilon_z^{\mathrm{EH}} & c\chi_z^{\mathrm{EH}} \\ c\chi_z^{\mathrm{EH}} & \mu_z^{\mathrm{EH}} \end{pmatrix}\begin{pmatrix} \sqrt{\epsilon_0}E_z \\ \sqrt{\mu_0}H_z \end{pmatrix}, \tag{20}$$

$$\xi = \frac{\epsilon_p^{\mathrm{EH}}}{\epsilon_p^{\mathrm{EH}}\mu_p^{\mathrm{EH}} - (c\chi_p^{\mathrm{EH}})^2 - (c\chi_o^{\mathrm{EH}})^2}, \tag{21}$$

$$\eta = \frac{\mu_p^{\mathrm{EH}}}{\epsilon_p^{\mathrm{EH}}\mu_p^{\mathrm{EH}} - (c\chi_p^{\mathrm{EH}})^2 - (c\chi_o^{\mathrm{EH}})^2}, \tag{22}$$

$$\tilde{\chi}_p = \frac{c\chi_p^{\mathrm{EH}}}{\epsilon_p^{\mathrm{EH}}\mu_p^{\mathrm{EH}} - (c\chi_p^{\mathrm{EH}})^2 - (c\chi_o^{\mathrm{EH}})^2}, \tag{23}$$

$$\tilde{\chi}_o = \frac{c\chi_o^{\mathrm{EH}}}{\epsilon_p^{\mathrm{EH}}\mu_p^{\mathrm{EH}} - (c\chi_p^{\mathrm{EH}})^2 - (c\chi_o^{\mathrm{EH}})^2}. \tag{24}$$

The ME coupling of Eq. (5) is a generic form with rotational symmetry. Here, we categorize the ME couplings into uniaxial and off-diagonal types. In the former type, $\chi_o = 0$, whereas in the latter type, $\chi_p = \chi_z = 0$. In what follows, we discuss the two types separately.

2.1 Off-diagonal magnetoelectric media

In the off-diagonal ME media, if the duality is met ($\epsilon_p^{\mathrm{EH}} = \mu_p^{\mathrm{EH}}$ and $\epsilon_z^{\mathrm{EH}} = \mu_z^{\mathrm{EH}}$), we have $\xi = \eta$. In this case, the Maxwell equation is decoupled into left and right circular-polarized components as

$$-\boldsymbol{\nabla}\cdot(\xi\boldsymbol{\nabla}\psi_L) - i[\boldsymbol{\nabla}\times(\tilde{\chi}_o\boldsymbol{\nabla}\psi_L)]_z = \frac{\omega^2}{c^2}\epsilon_z^{\mathrm{EH}}\psi_L, \tag{25}$$

$$-\boldsymbol{\nabla}\cdot(\xi\boldsymbol{\nabla}\psi_R)+i[\boldsymbol{\nabla}\times(\tilde{\chi}_o\boldsymbol{\nabla}\psi_R)]_z=\frac{\omega^2}{c^2}\epsilon_z^{\rm EH}\psi_R, \tag{26}$$

$$\psi_L=\sqrt{\epsilon_0}E_z+i\sqrt{\mu_0}H_z,\quad \psi_R=i\sqrt{\epsilon_0}E_z+\sqrt{\mu_0}H_z. \tag{27}$$

At $\tilde{\chi}_o=0$, the equations for the L and R modes are the same.

The above equations are formally the same as the Maxwell equation for the transverse-magnetic (TM) [or transverse-electric (TE)] polarization in a magneto-optical medium of the permeability (or permittivity):

$$-\boldsymbol{\nabla}\cdot(\xi_{\rm MO}\boldsymbol{\nabla}E_z)-i[\boldsymbol{\nabla}\times(\zeta_{\rm MO}\boldsymbol{\nabla}E_z)]_z=\frac{\omega^2}{c^2}\epsilon_z E_z, \tag{28}$$

$$\xi_{\rm MO}=\frac{\mu_p}{\mu_p^2-\kappa^2},\quad \zeta_{\rm MO}=-\frac{\kappa}{\mu_p^2-\kappa^2},\quad \overleftrightarrow{\mu}=\begin{pmatrix}\mu_p & i\kappa & 0\\ -i\kappa & \mu_p & 0\\ 0 & 0 & \mu_z\end{pmatrix}. \tag{29}$$

Here, the magneto-optical coupling κ is proportional to the applied magnetic field or spontaneous magnetization. Therefore, our system with the ME coupling is mapped to the magneto-optical system in which the L and R modes are subjected to an opposite (antiparallel) magnetic field. This mapping is reminiscent of the Kane-Mele model,[21] in which the up and down spins are subjected to the antiparallel magnetic fields owing to the spin-orbit interaction.

Here, we can introduce a fermionic time-reversal operation $\mathcal{T}_f$ as

$$\mathcal{T}_f\begin{pmatrix}\sqrt{\epsilon_0}E_z(\boldsymbol{x})\\ \sqrt{\mu_0}H_z(\boldsymbol{x})\end{pmatrix}\equiv\begin{pmatrix}\sqrt{\mu_0}H_z^*(\boldsymbol{x})\\ -\sqrt{\epsilon_0}E_z^*(\boldsymbol{x})\end{pmatrix}, \tag{30}$$

which satisfies $\mathcal{T}_f^2=-1$ and is written as $\mathcal{T}_f=i\hat{\sigma}_y\mathcal{K}$. Here, $\hat{\sigma}_i$ $(i=x,y,z)$ is the Pauli matrix and $\mathcal{K}$ is the complex conjugation operator. The system with the electromagnetic duality is invariant under $\mathcal{T}_f$. On the other hand, the conventional (bosonic) time-reversal operation $\mathcal{T}_b$ is given by

$$\mathcal{T}_b\begin{pmatrix}\sqrt{\epsilon_0}E_z(\boldsymbol{x})\\ \sqrt{\mu_0}H_z(\boldsymbol{x})\end{pmatrix}\equiv\begin{pmatrix}\sqrt{\epsilon_0}E_z^*(\boldsymbol{x})\\ -\sqrt{\mu_0}H_z^*(\boldsymbol{x})\end{pmatrix}, \tag{31}$$

which satisfies $\mathcal{T}_b^2=1$, and is written as $\mathcal{T}_b=\hat{\sigma}_z\mathcal{K}$. This symmetry is broken because of nonzero $\tilde{\chi}_o$.

The fermionic TRS causes the Kramers degeneracy. Since we are considering a periodic system, as shown in Fig. 1, photonic eigenstates are characterized by momentum $\boldsymbol{k}$ in the first Brillouin zone. The fermionic TRS to our system implies

$$\omega_L(-\boldsymbol{k})=\omega_R(\boldsymbol{k}), \tag{32}$$

resulting in the Kramers degeneracy between L and R modes at time-reversal invariant momenta. Besides, if the system has the SIS, namely, $\theta(-\boldsymbol{x})=\theta(\boldsymbol{x})$ for $\theta=\xi,\epsilon_z,\tilde{\chi}_o$, then we have

$$\omega_L(-\boldsymbol{k})=\omega_L(\boldsymbol{k}),\quad \omega_R(-\boldsymbol{k})=\omega_R(\boldsymbol{k}). \tag{33}$$

Combining Eqs. (32) and (33), we obtain the double degeneracy between L and R modes in the entire Brillouin zone. If either the SIS or the fermionic TRS is broken, the double degeneracy is lifted.

Typical photonic band structures are shown in Fig. 2 for the triangular- and kagome-lattice PhCs with the electromagnetic duality and SIS. To clarify the roles of spatial anisotropy, we introduce different radii for the kagome lattice (but the SIS is preserved). The plane-wave expansion method[23] is employed for the photonic band calculation. Since all the bands are doubly degenerate, we have the quartic degeneracy at the Γ, K, and K' points in the first Brillouin zone for vanishing coupling χ_o in the triangular lattice. The quartic degeneracies at K and K' are of the Dirac type. These quartic degeneracies are lifted into two doubly degenerate modes for nonzero χ_o. As a result, all the bands are separated in frequency from each

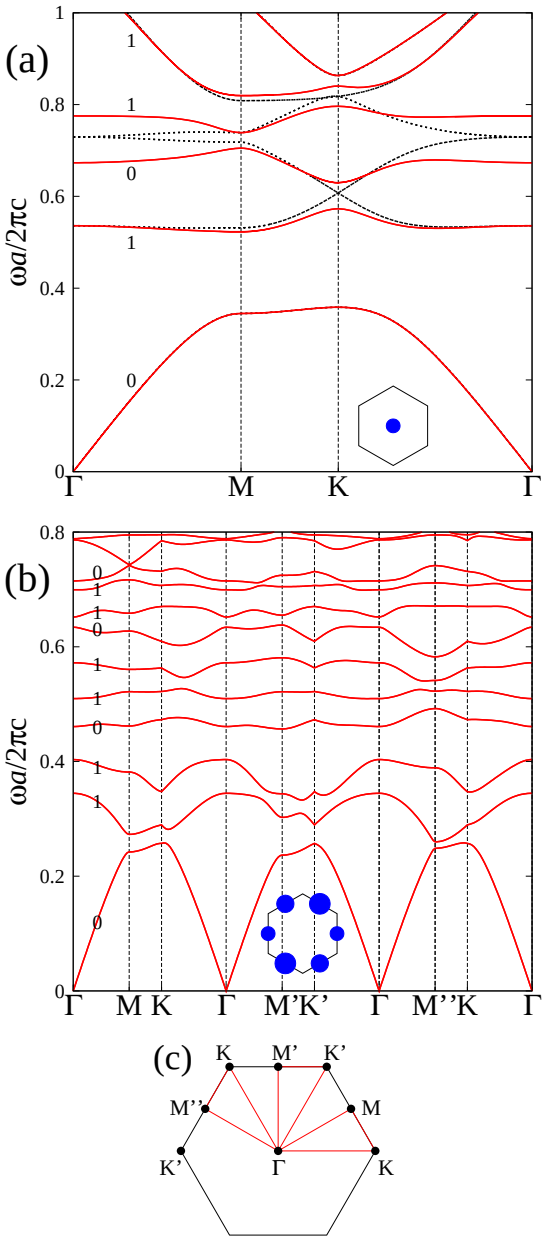

Fig. 2. (Color online) Photonic band structures of periodic arrays of circular cylinders with the off-diagonal magnetoelectric coupling are shown by solid lines. The background medium is air. All the bands are doubly degenerate. The following parameters are employed for the magnetoelectric medium (taken from Ref. 20 assuming a Bragg stack of piezoelectric and piezomagnetic layers): $\epsilon_p=2.5, \mu_p=5.714$, $\epsilon_z=\mu_z=14.2$, $\chi_o=0.75$ ($\epsilon_p^{\rm EH}=\mu_p^{\rm EH}=5.714$). The large magnetoelectric coupling χ_o corresponds to a value near the resonance of the elastic oscillation in the Bragg stack. Therefore, strictly speaking, the calculation is justified in a narrow frequency window near the resonance. (a) Triangular lattice. The radius of the rods is $0.1a$, where a is the lattice constant. (b) Kagome lattice. The radii are $0.125a$, $0.15a$, and $0.1a$. (c) First Brillouin zone and points of high symmetry. For comparison, the band structure with vanishing ME coupling ($\chi_o=0$) is also shown by dotted lines in (a). The Z_2 indices ν of the photonic bands, in which $(-1)^\nu$ is the product of the parities at the time-reversal invariant momenta (Γ, M, M', and M''), are also indicated. Insets show unit cells.

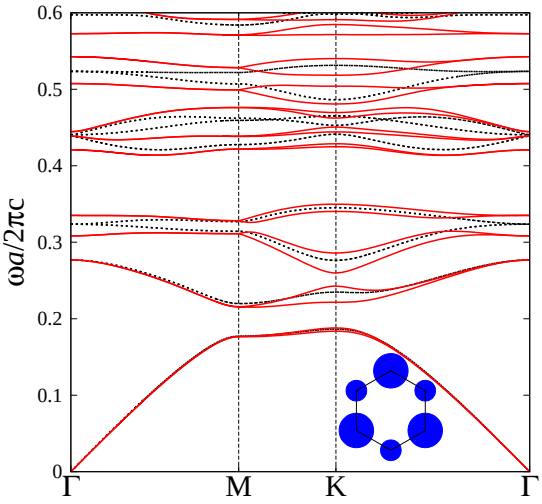

Fig. 3. (Color online) Photonic band structures of the honeycomb lattice of circular cylinders before (dotted line) and after (solid line) introducing the off-diagonal magnetoelectric coupling. The background medium is air. The same material parameters as in Fig. 2 are employed. The radii of the cylinders are taken to be $0.25a$ and $0.15a$, where a is the lattice constant. Inset shows a unit cell.

other. As for the kagome lattice, the quartic degeneracy is absent even at vanishing χ_o because of the spatial anisotropy.

In these systems, we can easily evaluate the Z_2 indices defined originally for the electronic band structure in TI.[24] The index ν is defined as

$$(-1)^{\nu} = \prod_{\boldsymbol{k}=\Gamma,\mathrm{M},\mathrm{M}',\mathrm{M}''} \sigma_P(\boldsymbol{k}), \tag{34}$$

where σ_P is the parity eigenvalue with respect to the space inversion. According to the bulk-edge correspondence of TI, if the sum of the Z_2 indices (modulo 2) of the bands below a gap is equal to 1, we obtain helical edge states in the gap. The edge states are robust against $\mathcal{T}_f$-preserving perturbations, but are fragile against $\mathcal{T}_f$ breaking perturbations. The calculated Z_2 indices suggests that the helical edge states are formed in the gaps between the second and third bands and the third and fourth bands for the triangular lattice, and the gaps between the fifth and sixth bands and the eighth and ninth bands for the kagome lattice. We will see in Sect. 4 that this is the case.

As an example of the system without the SIS, Fig. 3 shows the photonic band structure of a honeycomb-lattice PhC. In this case, the double degeneracy in the entire Brillouin zone no longer holds at nonzero χ_o. However, along the ΓM interval, the double degeneracy is observed. This is because of the parity symmetry with respect to the axis. Namely, we have $\theta(\sigma\boldsymbol{x}) = \theta(\boldsymbol{x})$ for $\theta = \xi, \epsilon_z, \tilde{\chi}_o$, where σ is the parity operation. Since the parity operation swaps the L and R modes, we immediately have

$$\omega_L(\sigma\boldsymbol{k}) = \omega_R(\boldsymbol{k}). \tag{35}$$

Therefore, if momentum $\boldsymbol{k}$ is invariant under the parity operation (e.g., on the ΓM interval), we have the degeneracy between L and R. The evaluation of the Z_2 indices is rather involved in this case. However, we can identify the gaps that hold helical edge states using an effective-hamiltonian argument given in the next section.

2.2 *Uniaxial magnetoelectric media*

In the uniaxial ME media, the duality does not cause the fermionic TRS. Instead, a bosonic TRS other than the conventional one can be introduced:

$$\mathcal{T}_b' \begin{pmatrix} \sqrt{\epsilon_0}E_z(\boldsymbol{x}) \\ \sqrt{\mu_0}H_z(\boldsymbol{x}) \end{pmatrix} \equiv \begin{pmatrix} \sqrt{\epsilon_0}H_z^*(\boldsymbol{x}) \\ \sqrt{\mu_0}E_z^*(\boldsymbol{x}) \end{pmatrix}. \tag{36}$$

However, it does not yield the Kramers degeneracy because $\mathcal{T}_b'^2 = 1$.

To introduce a fermionic TRS, we need to assume the antiduality $\epsilon_p^{\mathrm{EH}} = -\mu_p^{\mathrm{EH}}$ ($\xi = -\eta$) and $\epsilon_z^{\mathrm{EH}} = -\mu_z^{\mathrm{EH}}$. The Maxwell equation is then decoupled into L and R polarization sectors as

$$-\boldsymbol{\nabla}\cdot((\xi - i\tilde{\chi}_p)\boldsymbol{\nabla}\psi_L) = \frac{\omega^2}{c^2}(\epsilon_z^{\mathrm{EH}} - ic\chi_z^{\mathrm{EH}})\psi_L, \tag{37}$$

$$-\boldsymbol{\nabla}\cdot((\xi + i\tilde{\chi}_p)\boldsymbol{\nabla}\psi_R) = \frac{\omega^2}{c^2}(\epsilon_z^{\mathrm{EH}} + ic\chi_z^{\mathrm{EH}})\psi_R. \tag{38}$$

The fermionic TRS $\mathcal{T}_f = i\hat{\sigma}_y\mathcal{K}$ and the SIS result in the double degeneracy in the entire Brillouin zone. However, such an antidual medium screens the radiation field everywhere in space, and we could not find any example that exhibits photonic bands in the frequency range $0 < \omega a/2\pi c < 1$.

3. Effective Hamiltonian

In the previous section, we presented PhC structures with ME couplings as a photospin-orbit interaction. The electromagnetic duality enables us to introduce the fermionic TRS from which the Kramers degeneracy is derived in a photonics platform. These items along with the Dirac-cone dispersions in triangular, honeycomb, and kagome lattices can be used to imitate the Kane-Mele model of the two-dimensional TI. Its effective hamiltonian is given by

$$\mathcal{H}_{\mathrm{KM}} = v(\tau_z\hat{\sigma}_x k_x + \hat{\sigma}_y k_y) + s_z\tau_z\hat{\sigma}_z M. \tag{39}$$

Here, $\tau_z(=\pm 1)$ is the valley spin, and $s_z(=\pm 1)$ is the real spin. It has energy eigenvalues $\mathcal{E} = \pm\sqrt{v^2\boldsymbol{k}^2 + M^2}$ regardless of the valley and real spins. Therefore, in a given valley of K or K', eigenmodes are doubly degenerate with respect to the real spin. We found that only the case of the off-diagonal ME coupling with the SIS is mapped to the Kane-Mele model modulo unitary transformation.

Let us consider the plane-wave-expansion form of Eqs. (25) and (26):

$$\sum_{\boldsymbol{g}'}\Big\{\xi_{\boldsymbol{g}-\boldsymbol{g}'}(\boldsymbol{k}+\boldsymbol{g})\cdot(\boldsymbol{k}+\boldsymbol{g}') + is_z\tilde{\chi}_{o;\boldsymbol{g}-\boldsymbol{g}'}[(\boldsymbol{k}+\boldsymbol{g})\times(\boldsymbol{k}+\boldsymbol{g}')]_z\Big\}\psi_{\boldsymbol{g}'} = \frac{\omega^2}{c^2}\sum_{\boldsymbol{g}'}\epsilon_{z;\boldsymbol{g}-\boldsymbol{g}'}^{\mathrm{EH}}\psi_{\boldsymbol{g}'}, \tag{40}$$

$$\psi(\boldsymbol{x}) = \sum_{\boldsymbol{g}} e^{i(\boldsymbol{k}+\boldsymbol{g})\cdot\boldsymbol{x}}\psi_{\boldsymbol{g}}, \tag{41}$$

$$\theta(\boldsymbol{x}) = \sum_{\boldsymbol{g}} e^{i\boldsymbol{g}\cdot\boldsymbol{x}}\theta_{\boldsymbol{g}} \quad (\theta = \xi, \tilde{\chi}_o, \epsilon_z^{\mathrm{EH}}). \tag{42}$$

Here, we introduce the real-spin index s_z, which is 1 for L and -1 for R polarization. Since the equation is formally the same as in the magneto-optical PhC, we can borrow the idea of the effective hamiltonian applied to the magneto-optical PhC.

The effective hamiltonian around the degenerate points in the Brillouin zone was constructed explicitly by the present author in Appendices of Ref. 25. For the triangular lattice, the effective hamiltonian around the corner and the center of the first Brillouin zone becomes

$$\mathcal{H}_{\mathrm{K(K')}} = v\tau_z(\hat{\sigma}_z\delta k_x - \hat{\sigma}_x\delta k_y) + s_z c_\chi \chi_o \hat{\sigma}_y, \tag{43}$$

$$\mathcal{H}_\Gamma = (c_1|\boldsymbol{k}|^2 + c_2\chi_o^2)\hat{1} + c_3 s_z \chi_o \hat{\sigma}_y + c_4[(k_x^2 - k_y^2)\hat{\sigma}_z + 2k_x k_y \hat{\sigma}_x], \tag{44}$$

where the coefficients v, c_χ, and c_i ($i = 1, 2, 3, 4$) are determined with the unperturbed eigenstates at the degenerate points. The deviation of the wavevector $\delta\boldsymbol{k}$ is measured from the K (or K ') point. The eigenvalues of the effective hamiltonians become

$$\mathcal{E}_{\mathrm{K(K')}} = \pm\sqrt{v^2|\delta\boldsymbol{k}|^2 + (c_\chi\chi_o)^2}, \tag{45}$$

$$\mathcal{E}_\Gamma = c_1|\boldsymbol{k}|^2 + c_2\chi_o^2 \pm \sqrt{c_4^2|\boldsymbol{k}|^4 + (c_3\chi_o)^2}, \tag{46}$$

resulting in the gapped dispersions. Note that the band gap in the Dirac cone becomes a true band gap (regardless of $\delta\boldsymbol{k}$) if the Dirac point at K (or K') is frequency-isolated. It gives the band width of the helical edge states or resulting helical optical waveguide.

The Chern number (for a given spin) caused by the Dirac hamiltonian is given by the parity-anomaly form:[25,26]

$$C = \frac{1}{2}(\mathrm{sgn}M_{\mathrm{K}} + \mathrm{sgn}M_{\mathrm{K'}}) = \mathrm{sgn}(s_z c_\chi \chi_o) \tag{47}$$

$$(M_{\mathrm{K}} = M_{\mathrm{K'}} = s_z c_\chi \chi_o), \tag{48}$$

if the relevant bands are touched solely at the K and K' points. In the quadratic hamiltonian the Chern number is given by

$$C = \mathrm{sgn}(s_z c_3 \chi_o). \tag{49}$$

In both cases, the "charge" Chern number $C_L + C_R$ vanishes, whereas the spin Chern number $(C_L - C_R)/2$ becomes nonzero, $\mathrm{sgn}(c_{\chi(3)}\chi_o)$. Accordingly, the helical edge states are expected to emerge in the relevant gaps. Such gaps are found in Fig. 2(a) (the gaps between the 2nd and 3rd and between the 3rd and 4th bands), although the relevant bands are touched at both Γ and K (K') for vanishing χ_o. The relevant Z_2 indices are consistent with the spin Chern number.

As for the kagome lattice, we assume different cylinder radii in Fig. 2(b) to see the roles of the spatial anisotropy. There, even if the ME coupling vanishes, we do not have the quartic degeneracy in the entire Brillouin zone. However, if all the cylinders are identical, we also have the quartic degeneracy at Γ, K, and K'. The $\boldsymbol{k}\cdot\boldsymbol{p}$ perturbation and the perturbation of the ME coupling from the degenerate points give the same effective hamiltonians as in the triangular lattice.

In the case of the honeycomb lattice without the SIS, nontrivial topology emerges from the quartic degeneracy at the Γ point. Therefore, the effective hamiltonian around the Γ point is relevant. The effective hamiltonian was also derived in Ref. 25 for magneto-optical PhCs. By applying it, we obtain

$$\mathcal{H}_\Gamma = (c_1|\boldsymbol{k}|^2 + c_2\chi_o^2)\hat{1} + \hat{\sigma}_y s_z c_3 \chi_o + \hat{\sigma}_z(c_4(k_x^2 - k_y^2) + s_z c_5 \chi_o) + \hat{\sigma}_x(c_4 2k_x k_y - s_z c_5 \chi_o). \tag{50}$$

By diagonalizing the effective hamiltonian, we have a gapped dispersion

$$\mathcal{E}_\Gamma = c_1|\boldsymbol{k}|^2 + c_2\chi_o^2 \pm \sqrt{D_{\boldsymbol{k}}}, \tag{51}$$

$$D_{\boldsymbol{k}} = c_4^2|\boldsymbol{k}|^4 + (c_5\chi_o)^2|\boldsymbol{k}|^2 + 2c_4 c_5 \chi_o k_x(k_x^2 - 3k_y^2) + (c_3\chi_o)^2. \tag{52}$$

The Chern number (for a given spin) is evaluated as

$$C = \mathrm{sgn}(s_z c_3 \chi_o). \tag{53}$$

Therefore, the charge and spin Chern numbers are equal to 0 and $\mathrm{sgn}(c_3\chi_o)$, respectively, suggesting helical edge states in the gap. Such gaps are found in Fig. 3 around $\omega a/2\pi c = 0.32$ and 0.51.

4. Edge States

In this section, we consider photonic edge states in the off-diagonal ME PhCs with and without the SIS. To prevent possible edge states escaping from the PhCs, we introduce a cladding by screened media.[27]

It is important to preserve the fermionic TRS also for the screened media. Otherwise, PTI is broken. This constraint implies that the electromagnetic duality must exist even in the screened media. Here, we take a rather artificial setup in which the permittivity and permeability of the screened medium are given by

$$\overleftrightarrow{\epsilon} = \overleftrightarrow{\mu} = \mathrm{diag}(1, 1, -1). \tag{54}$$

A conventional screened medium, such as the perfect electric conductor, breaks the fermionic TRS. Note that air is also a dual medium with $\overleftrightarrow{\epsilon} = \overleftrightarrow{\mu} = \overleftrightarrow{1}$.

The method employed in the evaluation of the edge states is the two-dimensional photonic Korringa-Kohn-Rostoker method.[28] We have extended the method to deal with cylinders with the ME coupling. The basic algorithm is reported in Refs. 29 and 30.

Figure 4 shows the dispersion relation of the edge state in the triangular- and kagome-lattice PhCs, cladded by the dual medium. We can see clearly gapless edge states in the bulk-band gaps around $\omega a/2\pi c = 0.6$ and 0.72 in Fig. 4(a), and around $\omega a/2\pi c = 0.68$ in Fig. 4(b).[31] The relevant Z_2 indices of the gaps are 1. Therefore, the bulk-edge correspondence is fulfilled. The edge states are shown to be helical by evaluating their polarization properties. Moreover, the dispersion curves of the edge states cross at a time-reversal invariant momentum ($k_\parallel = 0$). The crossing is due to the Kramers degeneracy for the edge states. Therefore, it is protected by the fermionic TRS.

As for the gap around $\omega a/2\pi c = 0.8$ in Fig. 4(a), we have two pairs of the helical edge states. These edge states are not robust against possible perturbations that mix the L and R modes but preserve the fermionic TRS. Although the Kramers degeneracy prohibits a gap opening at the crossing point of $k_\parallel a/2\pi = \pm 0.5$, the crossing at about $k_\parallel a/2\pi = \pm 0.4$ yields a gap by the perturbation. Resulting edge states are gapped.

Figure 5 shows the field configuration of the helical edge state at the marked point p_1 in Fig. 4(a). Since the mode under consideration is inside the light cone ($\omega > c|k_\parallel|$), it has the small imaginary part (inversely proportional to the Q factor) in the eigenfrequency. As a result, the mode can be excited

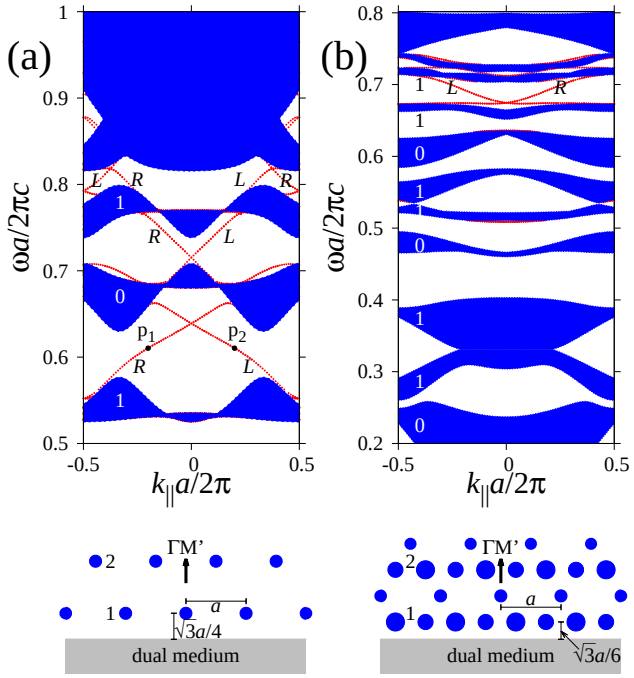

Fig. 4. (Color online) Dispersion relation of the edge states in the (a) triangular- and (b) kagome-lattice photonic crystal stripes. Edge geometries are shown in the lower panels. The same parameters as in Fig. 2 are employed for the photonic crystal in the bulk. The photonic crystal stripe consists of an 8-layer stack in the ΓM' direction. One side of the stripe is cladded by the dual medium of $\overleftrightarrow{\epsilon} = \overleftrightarrow{\mu} = \mathrm{diag}(1,1,-1)$ with semi-infinite thickness. The other side is tangent to air ($\overleftrightarrow{\epsilon} = \overleftrightarrow{\mu} = \overleftrightarrow{1}$). The shaded region stands for the projection of the bulk band structure. Dots represent the edge states localized near the clad side. Polarization (either L or R) of the edge states and the Z_2 indices of the bulk bands are also indicated. Lower panels show the edge geometries.

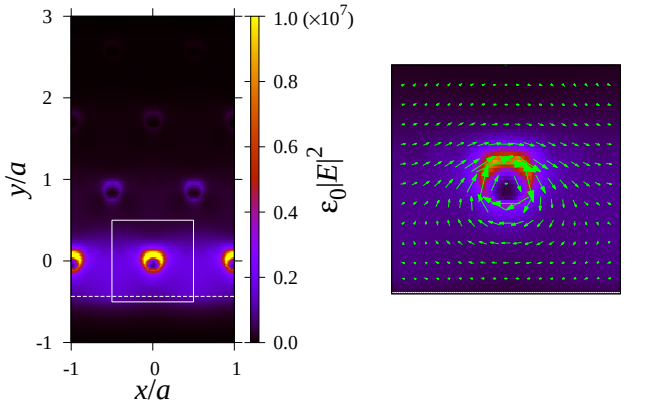

Fig. 5. (Color online) Field configuration of the edge states at the marked point (p_1; $k_\parallel a/2\pi = -0.2$) in Fig. 4(a). The absolute square of the electric field is plotted. The edge state is excited by the incident plane wave coming from the top of the structure (8-layer stack in the ΓM' direction). The z components of the incident electromagnetic field are given by $(\sqrt{\epsilon_0}E_z,\ \sqrt{\mu_0}H_z) = (1,i)/\sqrt{2}\exp(i\boldsymbol{k}\cdot\boldsymbol{x})$ with $\boldsymbol{k} = \left(k_\parallel, -\sqrt{(\omega/c)^2 - k_\parallel^2}\right)$. The dashed line in the left panel stands for the cladding interface. The right panel shows the magnified view of the field configuration in the square region of the left panel, overlaid by the Poynting vector flow.

by an incident light with a fine-tuned frequency. Actually, in the simulation, a plane wave is incident on the structure from the top (air side). The edge states are excited selectively by the polarization of the incident light. If it is circular-polarized with

$$(\sqrt{\epsilon_0}E_z,\ \sqrt{\mu_0}H_z) = \frac{1}{\sqrt{2}}(1,\pm i)e^{i\boldsymbol{k}\cdot\boldsymbol{x}}, \tag{55}$$

$$\boldsymbol{k} = \left(k_\parallel, -\sqrt{\frac{\omega^2}{c^2} - k_\parallel^2}\right), \tag{56}$$

the mode at p_1 in Fig. 4(a) is excited by the $(1,+i)$ polarization. The Poynting vector flows clockwise around the cylinder. The mode at p_2 in Fig. 4(a) is its time-reversal partner and can be excited by the $(1,-i)$ polarization. The Poynting vector flow is now counter-clockwise (not shown).

To explore the properties of the helical edge states, we consider two other types of edge termination in the triangular-lattice PhC, aside from that shown in Fig. 4(a). One is the edge normal to the ΓK direction with the cladding by the dual medium. The other is the edge normal to the ΓM' direction, but the cladding is now replaced by the perfect electric conductor. Figure 6 shows the corresponding edge-state spectra. Emergence of the helical edge states is not modified for the edge normal to ΓK, as shown in Fig. 6(a). However, if the cladding is by the perfect conductor, gaps open for the edge states. This is because $\mathcal{T}_f$ is broken by the boundary condition

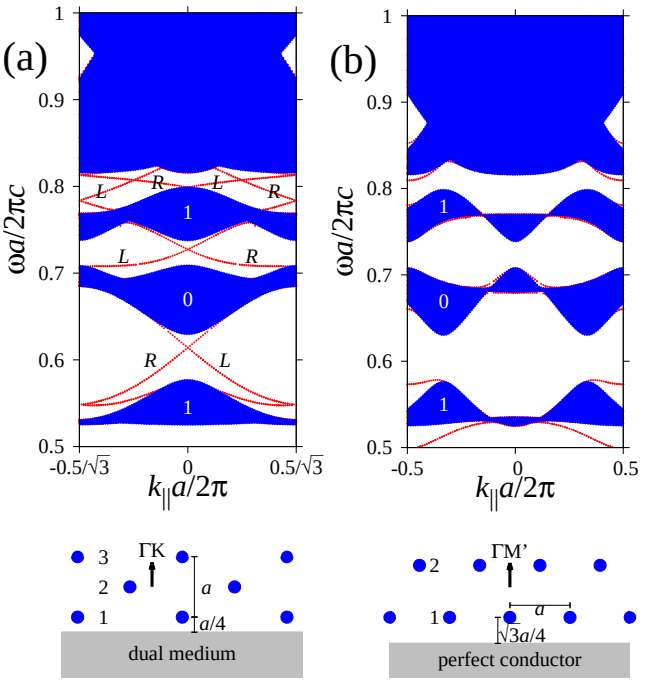

Fig. 6. (Color online) Dispersion relation of the edge states in the triangular-lattice photonic crystal stripes. The same parameters as in Fig. 2(a) are employed. The stripes consist of (a) a 16-layer stack in the ΓK direction cladded by the dual medium, and (b) an 8-layer stack in the ΓM' direction cladded by the perfect electric conductor. The shaded region stands for the projection of the bulk band structure. Dots indicate the edge states. Polarization of the edge states and the Z_2 indices of the bulk bands are also indicated. Lower panels show the edge geometries.

$\boldsymbol{E}_\parallel = 0$ of the perfect conductor. In addition, the edge states are not purely L- or R-polarized.

Finally, we consider the honeycomb-lattice PhC without the SIS. In this case, the nontrivial topology stems from the band-gap opening at the Γ point. Figure 7 shows the edge-state spectra. The relevant band gaps are around $\omega a/2\pi c =$

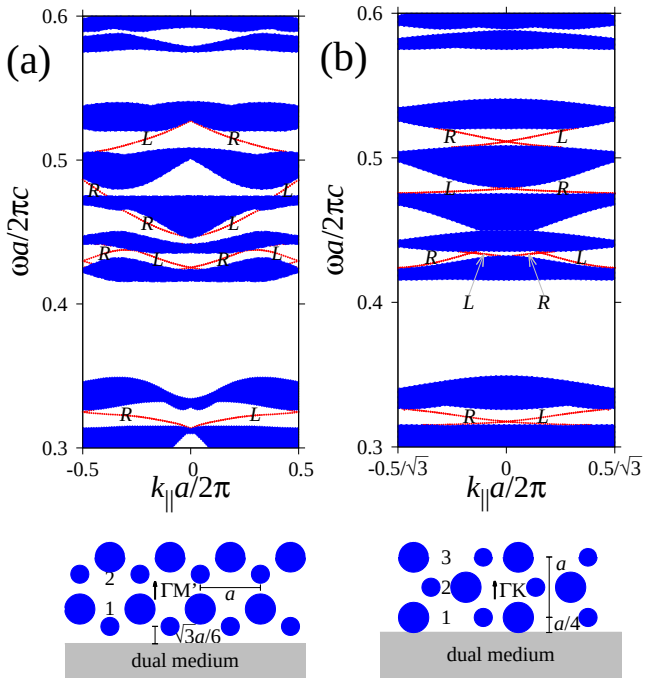

Fig. 7. (Color online) Dispersion relation of the edge states in the honeycomb-lattice photonic crystal stripes. The same parameters as in Fig. 3 are employed. The photonic crystal consists of (a) an 8-layer stack in the ΓM' direction and (b) a 16-layer stack in the ΓK direction. The shaded region stands for the projection of the bulk band structure. Dots represent the edge states. Polarization of the edge states (L or R) is indicated. Lower panels show the edge geometries.

0.32 and 0.51. We can see clearly the helical edge states there, as predicted by the effective hamiltonian. Besides, we have helical edge states in the gaps around $\omega a/2\pi c = 0.43$ and 0.48. If we closely look at the former gap, we find two pairs of the helical edge states, and the dispersion curves cross at time-reversal non-invariant momenta. Therefore, the helical edge states concerned are not robust. On the other hand, in the latter gap, we have a single pair of the helical edge states. They are not simply caused by the gap opening at the Γ point. Rather, they are strongly affected by the gap opening at the K and K' points because the relevant bulk bands are crowded there (see also Fig. 3). A band inversion in the two-parameter space spanned by the difference in the rod radii and the ME coupling is supposed to occur there.

5. Summary and Discussion

In summary, we have presented a detailed theoretical analysis on the PTIs in the PhCs with the ME coupling of the Tellegen type. If the coupling is off-diagonal and if the electromagnetic duality is met, the system is equivalent to a photospin-dependent magneto-optical system. The SIS results in a direct mapping of the system into the Kane-Mele model of TI, around the Brillouin zone corner. As a result, we can realize PTIs with helical edge states in the systems without conventional TRS. Even if the SIS is broken, PTI emerges. It originates from the gap opening around the Γ point by the photospin-orbit interaction of the ME coupling. These results are fully consistent among the Z_2 indices of the bulk photonic bands, the spin Chern numbers via the effective hamiltonian, and the edge-state characterizations.

In our model of PTI, the roles of the fermionic TRS are highlighted, because the bosonic TRS is broken. In contrast, the metamaterial model of PTI[8] has both the bosonic and fermionic TRS. The robustness of the PTI is protected by the latter symmetry, although there seems to be confusion about this issue, as discussed below.

We have various difficulties in realizing PTIs experimentally. The most serious problem is the electromagnetic duality. With the aid of the duality, the TE and TM modes are degenerate. Therefore, the ME coupling gives a strong perturbation to the system. If the duality is absent, the perturbation is weak. Known multiferroic media do not have the duality. It is thus too optimistic to assume a single-domain medium as a constitutive material of realistic PTI. We are forced to deal with composite media.

One possibility is a composite of the piezoelectric and piezomagnetic media. The mechanical strain between the two media gives rise to an effective ME coupling that is controllable by the geometry of the composite. In addition, the coupling can be enhanced by a structural resonance. Strong piezoelectricity and piezomagnetism are usually realized in ferroelectric and ferrimagnetic media, respectively. Since ferroelectric and ferrimagnetic media have large permittivity and permeability, respectively, the effective permittivity can be the same order as the effective permeability. Suppose that the piezoelectric (piezomagnetic) medium has the volume fraction x $(1-x)$. Then, the effective permittivity and permeability are given by

$$\epsilon_{\rm eff} = x\epsilon_{\rm PE} + (1-x)\epsilon_{\rm PM}, \tag{57}$$

$$\mu_{\rm eff} = x\mu_{\rm PE} + (1-x)\mu_{\rm PM}, \tag{58}$$

where $\epsilon_{\rm PE(PM)}$ and $\mu_{\rm PE(PM)}$ are the permittivity and permeability of the piezoelectric (piezomagnetic) medium, respectively. By imposing $\epsilon_{\rm eff} = \mu_{\rm eff}$, we can find the appropriate volume fraction for the duality.[32]

Even if the duality is met, we need to have a sufficiently large ME coupling to create the photonic band gap that supports helical edge states. Known multiferroic materials and composites of piezoelectric and piezomagnetic media exhibit strong dispersions in their ME couplings. Away from possible resonance frequencies, their ME couplings are generally small. Therefore, we need to fine-tune the system such that the quartic degeneracies in the photonic band structure emerge near the resonance frequencies. Therefore, it is still challenging to realize the PTI.

Although fine tuning is necessary, it is instructive to consider the effects of detuning with respect to the electromagnetic duality and the resulting fermionic TRS. To this end, we employ the effective hamiltonian as in Sect. 3. For simplicity, we consider Dirac points at K and K' in the triangular, honeycomb, and kagome lattices without spatial anisotropy. If we neglect the detuning, the effective hamiltonian around the Dirac point is given by Eq. (43). Introducing the detuning between permittivity and permeability gives rise to an additional term in the effective hamiltonian as

$$\Delta\mathcal{H}_{\rm K(K')} = \delta_D \hat{s}_y \otimes \hat{1}, \tag{59}$$

$$\delta_D = c_p(\epsilon_p^{\rm EH} - \mu_p^{\rm EH}) + c_z(\epsilon_z^{\rm EH} - \mu_z^{\rm EH}), \tag{60}$$

where $\hat{s}_i$ is the i-th component of the Pauli matrix acting on

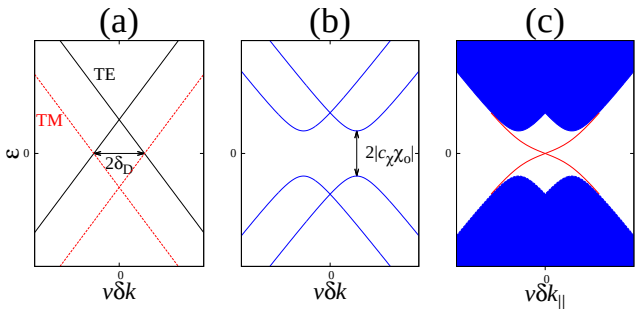

Fig. 8. (Color online) Effects of the detuning δ_D between permittivity and permeability, in terms of the effective hamiltonian around the Dirac point. (a) Energy spectrum before introducing the off-diagonal magnetoelectric coupling χ_o. The TE and TM polarizations are decoupled, and two Dirac points are found at $\delta\boldsymbol{k} = 0$. (b) Spectrum after introducing the magnetoelectric coupling. The TE and TM polarizations mix, forming a band gap. The Dirac-point degeneracies remain unlifted. (c) Dispersion relation of domain wall states. The domain wall separating two PhCs with opposite χ_o supports two domain-wall states with nearly gapless dispersion curves. The band crossing of the domain-wall states is due to the pseudo-time-reversal symmetry. The ratio $c_\chi\chi_o/\delta_D$ is taken to be $2/3$.

the real-spin space, and $\hat{1}$ is the 2 by 2 identity matrix acting on the pseudospin space (relevant to the upper and lower cones of the Dirac spectrum). The coefficients c_p and c_z are determined from the degenerate wave functions at the Dirac point. The valley dependence is absent in the additional term. Including this term results in four eigenvalues of the effective hamiltonian:

$$\mathcal{E} = \pm\sqrt{(v|\delta\boldsymbol{k}| + \delta_D)^2 + (c_\chi\chi_0)^2}, \quad \pm\sqrt{(v|\delta\boldsymbol{k}| - \delta_D)^2 + (c_\chi\chi_0)^2}. \tag{61}$$

The energy spectrum exhibits the band gap of width $2|c_\chi\chi_o|$, regardless of the detuning δ_D, as shown in Fig. 8. This gap supports possible edge states connecting two valleys of K and K', but the resulting edge states are no longer helical. Namely, the relevant edge states (such as in Figs. 4(a) and Fig. 6(a) around $\omega a/2\pi c = 0.6$) exhibit the band anticrossing at $k_\parallel = 0$ and become gapped. The gap width is proportional to the detuning. In addition, the two edge states (originally L and R polarized at zero detuning) are not paired by the fermionic TRS. Instead, they are E_z and H_z polarized at the anticrossing point. Therefore, the helical optical waveguiding in the bulk band gap is lost immediately after introducing the detuning.

However, the situation changes markedly when we consider a domain wall formed by two PhCs with opposite ME coupling χ_o as in Ref. 8. The above effective hamiltonian predicts two domain-wall states with nearly gapless dispersions inside the valley, as shown in Fig. 8(c). This is a generalization of the domain-wall fermion in the Dirac hamiltonian.[33] The dispersion curves cross at $\delta k_\parallel = 0$ regardless of the detuning. This is because of a pseudo-time-reversal symmetry the effective hamiltonian has. We can show that the effective hamiltonian is invariant under

$$\mathcal{T}_f^{\text{pseudo}} = i\hat{s}_x \otimes \hat{\sigma}_y\mathcal{K}, \tag{62}$$

regardless of the detuning. It maps $\delta\boldsymbol{k}$ to $-\delta\boldsymbol{k}$ (not as $\boldsymbol{k}$ to $-\boldsymbol{k}$, and thus we add "pseudo") and is fermionic $(\mathcal{T}_f^{\text{pseudo}})^2 = -1$. As a result, the Kramers degeneracy holds at the pseudo-time-reversal invariant momentum $\delta k_\parallel = 0$, and the domain-wall states are pseudo-helical (gapless and paired with the pseudo-time-reversal partners).

Nevertheless, in the entire $k_\parallel$ space, we can show via first-principles calculation that the domain-wall states are not gapless nor paired with the time-reversal partner. Actually, the dispersion curves of the domain-wall states do not traverse the band gap nor terminate in the different (upper and lower) bulk bands. This situation is quite similar to the domain-wall states found in the nonmagnetic honeycomb lattice PhC with Dirac spectrum.[30] There, the domain-wall states seem to be gapless inside a valley, but their dispersion curves do not traverse the gap. Thus, if the detuning is nonzero, the PTI is lost in a strict sense. However, the pseudo-TRS is emergent within the effective hamiltonian, resulting in the nearly gapless domain-wall states inside the K and K' valleys. A similar mechanism works in the metamaterial model of PTI.[8]

As explained, the electromagnetic duality gives rise to the fermionic TRS. This TRS is essential in our PTI. Besides, we also found that even if the duality is absent, it is possible to construct another fermionic TRS for honeycomb-lattice systems. Suppose we have two types of rods, namely, A and B rods in the honeycomb lattice. If the permittivity and permeability of the rods satisfy

$$\overleftrightarrow{\epsilon}_A^{\text{EH}} = \overleftrightarrow{\mu}_B^{\text{EH}}, \quad \overleftrightarrow{\mu}_A^{\text{TE}} = \overleftrightarrow{\epsilon}_B^{\text{TE}}, \tag{63}$$

with off-diagonal ME coupling with

$$\chi_{oA}^{\text{EH}} = \chi_{oB}^{\text{EH}} \tag{64}$$

or uniaxial ME coupling with

$$\chi_{pA}^{\text{EH}} = -\chi_{pB}^{\text{EH}}, \quad \chi_{zA}^{\text{EH}} = -\chi_{zB}^{\text{EH}}, \tag{65}$$

the system is invariant under a fermionic time-reversal operation defined by

$$\mathcal{T}_f'\begin{pmatrix} \sqrt{\epsilon_0}E_z(\boldsymbol{x}) \\ \sqrt{\mu_0}H_z(\boldsymbol{x}) \end{pmatrix} = \begin{pmatrix} \sqrt{\mu_0}H_z^*(-\boldsymbol{x}) \\ -\sqrt{\epsilon_0}E_z^*(-\boldsymbol{x}) \end{pmatrix}. \tag{66}$$

In this case, we do not need the electromagnetic duality in each rod. Instead, we just need the duality between A and B rods, which may be chosen from two different multiferroic media. Since $\mathcal{T}_f'$ does not change the momentum $\boldsymbol{k}$, the Kramers degeneracy is found in the entire Brillouin zone without assuming the SIS. Note that $\mathcal{T}_f'$ involves the space inversion. Therefore, the presence of an edge breaks explicitly this symmetry. However, if we consider a stripe shape, it is possible to preserve $\mathcal{T}_f'$. Although we could not find any evidence, it may be interesting to search for topological phenomena in such a system.

We hope that this paper stimulates further investigation on photonic topological insulators by ME media.

Acknowledgments

The author would like to thank the anonymous referee for valuable comments. This work was partially supported by JSPS KAKENHI (Grant No. 23540380).

1) M. Kohmoto, Ann. Phys. **160**, 343 (1985).
2) M. Z. Hasan and C. L. Kane, Rev. Mod. Phys. **82**, 3045 (2010).
3) M. Onoda, S. Murakami, and N. Nagaosa, Phys. Rev. Lett. **93**, 083901 (2004).
4) F. D. M. Haldane and S. Raghu, Phys. Rev. Lett. **100**, 013904 (2008).

5) Z. Wang, Y. D. Chong, J. D. Joannopoulos, and M. Soljačić, Nature **461**, 772 (2009).
6) J. Cho, D. G. Angelakis, and S. Bose, Phys. Rev. Lett. **101**, 246809 (2008).
7) V. Yannopapas, Phys. Rev. B **84**, 195126 (2011).
8) A. B. Khanikaev, S. H. Mousavi, W.-K. Tse, M. Kargarian, A. H. MacDonald, and G. Shvets, Nat. Mater. **12**, 233 (2013).
9) G. Q. Liang and Y. D. Chong, Phys. Rev. Lett. **110**, 203904 (2013).
10) M. C. Rechtsman, J. M. Zeuner, Y. Plotnik, Y. Lumer, D. Podolsky, F. Dreisow, S. Nolte, M. Segev, and A. Szameit, Nature **496**, 196 (2013).
11) K. Fang, Z. Yu, and S. Fan, Nat. Photon. **6**, 782 (2012).
12) M. Hafezi, S. Mittal, J. Fan, A. Migdall, and J. M. Taylor, Nat. Photon. **7**, 1001 (2013).
13) L. Lu, J. D. Joannopoulos, and M. Soljačić, Nat. Photon. **8**, 821 (2014).
14) I. V. Lindell, A. H. Sihvola, S. A. Tretyakov, and A. J. Viitanen: *Electromagnetic Waves in Chiral and Bi-isotropic Media* (Artech House, Norwood, 1994).
15) Y. B. Band: *Light and Matter: Electromagnetism, Optics, Spectroscopy and Lasers* (John Wiley & Sons, 2006), p. 142.
16) B. Tellegen, Philips Res. Rep **3**, 81 (1948).
17) W. Eerenstein, N. D. Mathur, and J. F. Scott, Nature **442**, 759 (2006).
18) J. Ryu, A. V. Carazo, K. Uchino, and H.-E. Kim, Jpn. J. Appl. Phys. **40**, 4948 (2001).
19) G. Srinivasan, E. T. Rasmussen, B. J. Levin, and R. Hayes, Phys. Rev. B **65**, 134402 (2002).
20) C. He, X.-C. Sun, X.-P. Liu, M.-H. Lu, Y. Chen, L. Feng, and Y.-F. Chen, arXiv:1405.2869 (2014).
21) C. L. Kane and E. J. Mele, Phys. Rev. Lett. **95**, 226801 (2005).
22) Exceptionally, if $\chi_p = \chi_z = 0$ and $\chi_o \neq 0$, in-plane parities are preserved. The z parity is broken.
23) M. Plihal and A. A. Maradudin, Phys. Rev. B **44**, 8565 (1991).
24) L. Fu and C. L. Kane, Phys. Rev. B **76**, 045302 (2007).
25) T. Ochiai, Phys. Rev. B **86**, 075152 (2012).
26) F. D. M. Haldane, Phys. Rev. Lett. **61**, 2015 (1988).
27) Since the photon energy is always positive, it is larger than the "vacuum" level. Therefore, without a screened medium the photon can escape from PhC through an edge if its frequency ω and wave number $k_\parallel$ parallel to the edge are inside the light cone $\omega > c|k_\parallel|$.
28) K. Ohtaka, T. Ueta, and K. Amemiya, Phys. Rev. B **57**, 2550 (1998).
29) T. Ochiai and M. Onoda, Phys. Rev. B **80**, 155103 (2009).
30) T. Ochiai, Int. J. Mod. Phys. B **28**, 1441004 (2014).
31) Concerning the narrow gap around $\omega a/2\pi c = 0.53$ in Fig. 4(b), we expect helical edge states from the Z_2 indices. However, since the gap is too narrow, the penetration depth of the relevant edge states becomes large. This fact prevents the formation of the helical edge states in the 8-layer-thick PhC. If the thickness is sufficiently large, we can observe the helical edge states.
32) Strictly speaking, this fraction is just for the in-plane component of permittivity and permeability. A correction term in the effective permittivity and permeability exists owing to the piezoelectric and piezomagnetic coupling. Moreover, we need to match the z component of the permittivity and permeability.
33) R. Jackiw and C. Rebbi, Phys. Rev. D **13**, 3398 (1976).